Bulletin of the Seismological Society of America, Vol. 73, No. 1, pp. 83–96, February 1983

A THEORETICAL STUDY OF THE RADIATION FROM SMALL STRIKE-SLIP EARTHQUAKES AT CLOSE DISTANCES

BY MICHEL CAMPILLO AND MICHEL BOUCHON

ABSTRACT

We present a study of the seismic radiation of a physically realistic source model—the circular crack model of Madariaga—at close distance range and for vertically heterogeneous crustal structures. We use this model to represent the source of small strike-slip earthquakes. We show that the characteristics of the radiated seismic spectra, like the corner frequency, are strongly affected by the presence of the free surface and by crustal layering, and that they can be considerably different from the ones of the homogeneous-medium far-field solution. The vertical and radial displacement spectra are the most strongly affected. We use this source model to calculate the decay of peak ground velocity with epicentral distance and source depth for small strike-slip earthquakes in California. For distances between 10 and 80 km, the peak horizontal velocity decay is of the form $r^{-1.25}$ for a 4-km hypocentral depth and $r^{-1.65}$ for deeper sources. The predominance of supercritically reflected arrivals beyond epicentral distances of 70 to 80 km produces a sharp change in the rate of decay of the ground motion. For most of the cases considered, the peak ground velocity increases between 80 and 100 km. We also show that the *S*-wave velocity in the source layer is the lower limit of phase velocities associated with significant ground motion.

INTRODUCTION

The continued growth over the past decade of microseismicity and aftershocks studies using magnetic tape recording has resulted in the collection of a considerable amount of data concerning small-size earthquakes. Because of the lag of theoretical modeling techniques, however, little of this huge quantity of information has been used. Although some attempts have been made to account for near-field seismic radiation and local crustal structure (Johnson and McEvilly, 1974; Helmberger and Malone, 1975; Helmberger and Johnson, 1977), most spectra of records obtained at very near distances from the source are still interpreted using models derived for the far-field and infinite homogeneous media.

Recent advances in numerical modeling techniques make it now possible to evaluate the complete seismic radiation of physically realistic source models at close distance range and for vertically heterogeneous crustal structures. The aim of this paper is to present such a technique. We shall show that the characteristics of the radiated seismic spectra can be drastically different from the ones of the homogeneous-medium far-field solution. As an application of the method, we shall calculate the decay of peak ground velocity with epicentral distance and source depth for small earthquakes in California. The ultimate goal of this paper is to encourage the use of such modeling techniques in aftershocks or microseismicity studies. We shall restrict the scope of this study to the case of strike-slip earthquakes.

SEISMIC SOURCE MODEL

It is now generally accepted that large seismic events are essentially composite. The barrier model (Aki *et al.*, 1977), for instance, represents the earthquake fault as a cluster of fractured patches separated by unbroken barriers. Ideally, a small

earthquake can be thought of as a single fractured patch. We shall represent such a source as a plane circular shear crack. We shall assume that rupture nucleates at a point and propagates radially at a constant velocity until it suddenly stops. The dynamics and far-field radiation of this model have been studied by Madariaga (1976). Recently, Archuleta and Hartzell (1981) have investigated its near-field radiation in a half-space. They have studied more specially the effects of fault finiteness and directivity.

Following Bouchon (1978), Boatwright (1980), and Archuleta and Hartzell (1981), we approximate the numerical solution for the slip time history on the fault (Madariaga, 1976) by an analytical approximation more suitable for calculation. Denoting by $\vec{r}$ the position vector from the center of the crack, we define the slip $\Delta u(\vec{r}, t)$ by the following expressions

$$\frac{\Delta u(\vec{r}, t)}{u_0} = 0 \qquad t < t_0(r),$$

$$\frac{\Delta u(\vec{r}, t)}{u_0} = \sqrt{V_r^2 t^2 - r^2} \qquad t_0(r) < t < t_1(r)$$

$$\frac{\Delta u(\vec{r}, t)}{u_0} = \sqrt{V_r^2 t_1(r)^2 - r^2} \qquad t > t_1(r) \tag{1}$$

with

$$t_0(r) = r/V_r, \qquad t_1(r) = R/V_r + (R - r)/V_h$$

$$u_0 = \frac{C\sigma_e}{\xi\mu}, \qquad \xi = 1 + V_r/V_h$$

where R is the source radius, β, V_r, and V_h are, respectively, the shear wave, rupture, and healing velocities, σ_e is the effective stress, μ is the shear modulus, and C is a numerical value depending on the rupture velocity to shear-wave velocity ratio.

In this model, the slip does not stop simultaneously on the fault. Once the rupture front stops, a healing wave propagates inward from the edge of the fault. Slip stops at the arrival of this wave. The initial part of the slip function (until the arrival of the P stopping phase) is identical to the solution obtained by Kostrov (1964) for a self-similar circular shear crack. It should be observed that this model introduces a discontinuity in the temporal evolution of slip velocity and a second order discontinuity in the final spatial distribution of slip.

Equations (1) allow us to calculate the far-field pulses and the associated spectral densities. Denoting by $\Delta\tilde{\dot{u}}(r, \omega)$, the Fourier transform of the slip velocity and by H the Hankel transform in the radial variable, the spectral density of the far-field pulse is given by (Madariaga, 1976)

$$\tilde{M}(\theta, \omega) = 2\pi\mu\Delta\hat{\tilde{\dot{u}}}(k, \omega)\,|_{k = (\omega \sin\theta)/v} \tag{2}$$

with

$$\Delta\hat{\tilde{\dot{u}}} \equiv H(\Delta\tilde{\dot{u}}(r, \omega))$$

and where v is, respectively, the P- or S-wave velocity depending on the type of wave considered, and θ is the azimuth of radiation measured from the normal to the fault plane.

In order to determine the healing velocity which best fits the dynamic solution, we compare the far-field P- and S-wave pulses radiated by our approximate analytic model with Madariaga's solution. We consider the same conditions as Madariaga ($V_r = 0.9\beta$) and compute the pulses radiated in azimuths of 0°, 45°, and 90° for two different healing velocities: the P-wave velocity (Figure 1A) and the S-wave velocity (Figure 1B). The best agreement with the dynamic solution for both signal duration and amplitude is obtained in the case of healing with the S-wave velocity. We shall, therefore, choose the shear-wave velocity as the healing velocity. Throughout this study, we shall assume a rupture velocity to shear-wave velocity ratio of 0.75.

The seismic moment associated with the source is defined by (Aki, 1966)

$$M_0 = \mu \int_0^R \int_0^{2\pi} \Delta u(r, t = \infty) r \, d\phi \, dr. \tag{3}$$

Using the expression of the slip in equation (1), we can perform the integration analytically, which yields

$$M_0 = 2\pi C \frac{\sigma_e}{\xi} R^3 \left(\frac{\xi^{1/2}(1 - \xi)}{2(2 - \xi)^{5/2}} \arccos(\xi - 1) + \frac{\xi^2}{3(2 - \xi)} + \frac{(1 - \xi)^2}{2(\xi - 2)^2} \right). \tag{4}$$

The corresponding local magnitude M_L can be estimated by applying the empirical relation

$$\log(M_0) = 1.5\, M_L + 16 \tag{5}$$

obtained by Thatcher and Hanks (1973) for southern California earthquakes.

Characteristics of Seismic Radiation

In order to compute the seismic radiation produced by the crack, we use the method proposed by Bouchon (1981) to calculate Green's functions in a layered half-space. We represent the extended circular source by a superposition of point sources. These individual sources are arranged in a rectangular network which covers the crack surface. The distance between neighboring sources is chosen to be much smaller than the shortest wavelength considered. The slip function depends on the position on the crack and is defined according to equations (1). We first consider the case of an elastic half-space characterized by P- and S-wave velocities of 6 and 3.5 km/sec and a density of 2.9 gm/cm^3. The source radius is 500 m and the hypocenter is at a depth of 4 km.

The surface displacements computed at epicentral distances of 2, 5, 10, and 25 km in a 60° azimuth with respect to the fault plane are shown in Figure 2. The interval between point sources is 50 m, and the frequency range extends from 0 Hz (static) to 10 Hz. The relative excitation of the different phases is similar to the one obtained by Israel and Kovach (1977) for a small strike-slip dislocation source.

At an epicentral distance of 2 km, the radial and vertical displacements are characterized by the absence of a well-defined P-wave pulse. The width of the S-wave pulse is similar to the one radiated in the far field. At a distance of 5 km, the P-wave pulse starts to develop. The SP head wave, which is radiated at the source as a shear wave and propagates along the surface as a P wave, is the major arrival on the radial component where it overshadows the S wave. At 10 and 25 km, the SP pulse is well separated from the S wave and is much larger than the S pulse on the

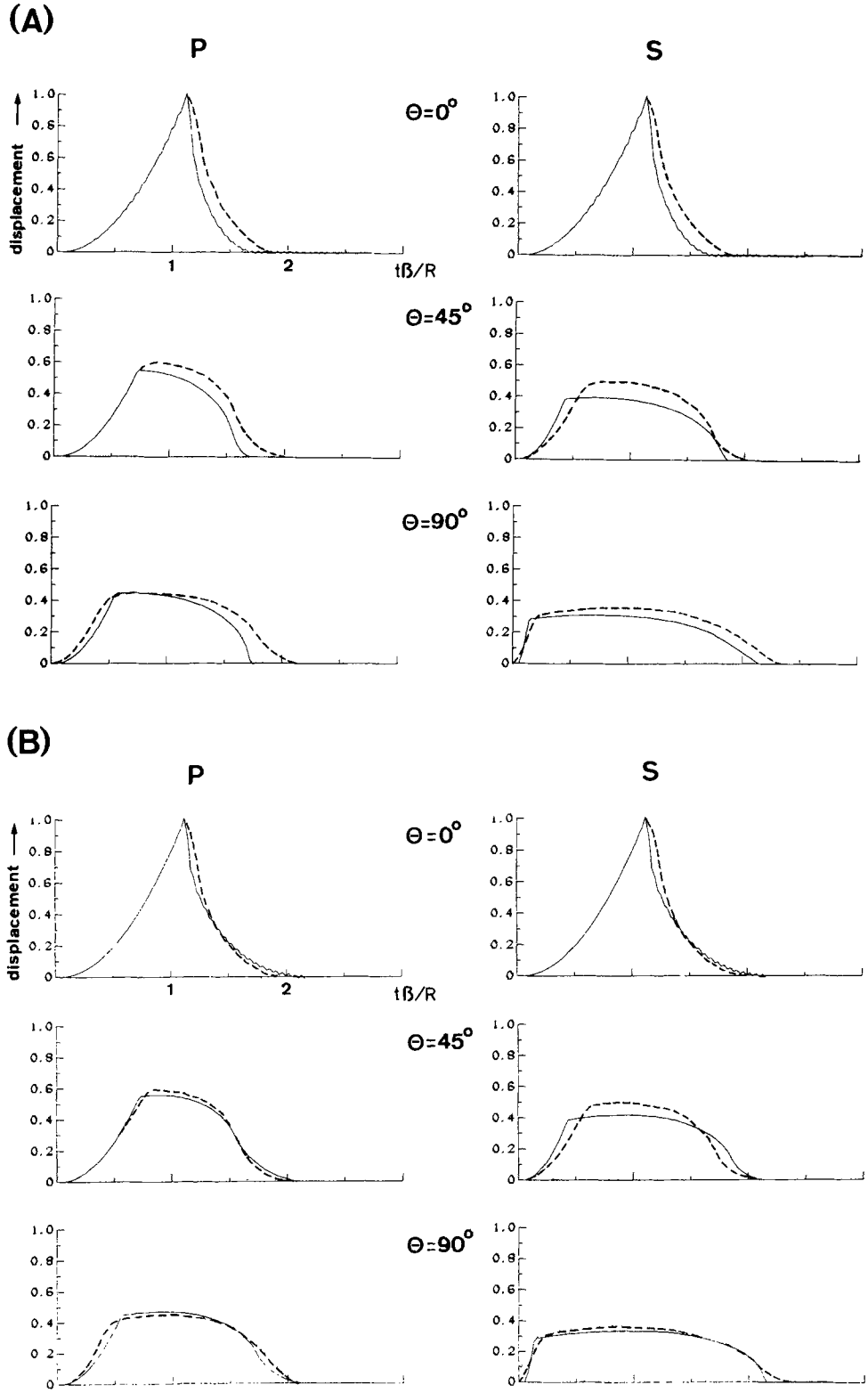

FIG. 1. Comparison between Madariaga's far-field displacement pulses and the ones obtained from analytical models with a healing phase propagating with P-wave velocity (A) and S-wave velocity (B). θ is measured with respect to the normal to the fault plane. Madariaga's solution is represented by the dashed line.

radial component. The *SP* wave also affects the vertical displacement. Another feature of the synthetics at this distance range is the appearance of the Rayleigh wave.

It is interesting to compare the evolution of the relative amplitudes of the three

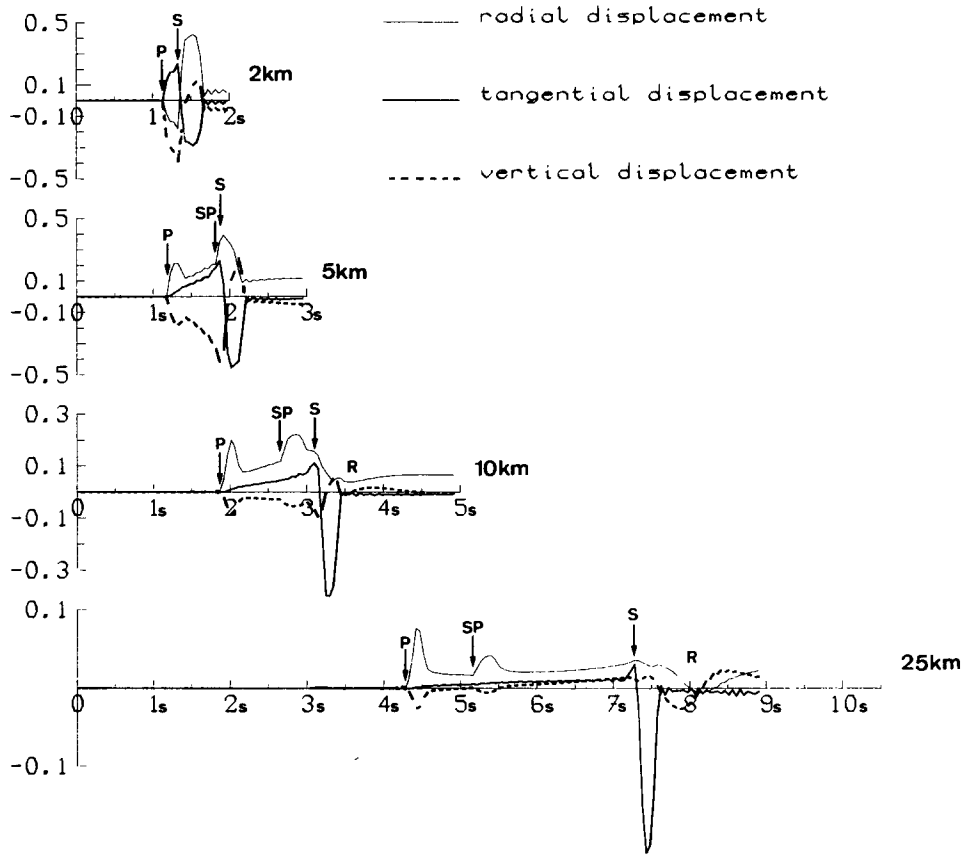

FIG. 2. Ground displacements at an azimuth of 60° and for different epicentral distances. The amplitude is given in centimeters for a 1-m displacement at the hypocenter.

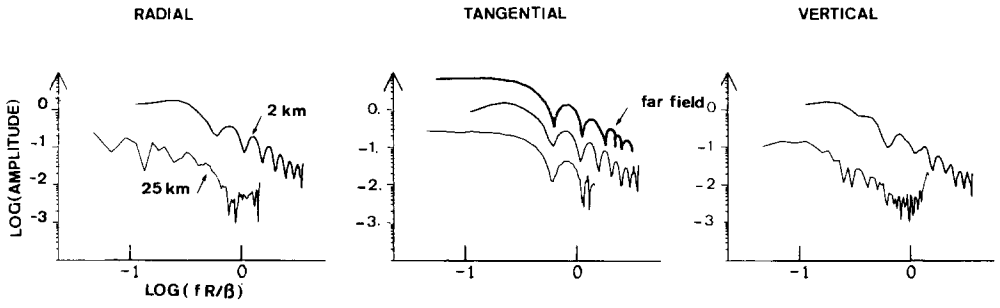

FIG. 3. Comparison of displacement spectra at different epicentral distances. The spectra are plotted as a function of nondimensional frequency fR/β.

components. At very close range, they are of comparable strength, but, as the epicentral distance increases, the transverse motion becomes more and more important.

Figure 3 shows a comparison between the displacement spectra obtained at epicentral distances of 2 and 25 km. The far-field *S*-wave displacement spectrum is

also presented. The frequency range considered extends to 25 Hz at 2 km and to 10 Hz at 25 km. The spectra of the transverse components at both distances are remarkably similar to the *S*-wave spectrum radiated in the far field. In particular, they display the same corner frequency and show the same rate of high-frequency decay. On the contrary, the spectral shapes of the radial and vertical components are strongly dependent on the epicentral distance considered. At 2 km distance, they are relatively close to the far-field displacement spectrum but become drastically different from it a 25 km. At this distance, the corner frequency, measured on the radial or vertical component, is a factor of 2 or 3 smaller than the one of the far-field *S* pulse. This implies that the evaluation of spectral source parameters, for strike-slip earthquakes, at least in the absence of strong vertical heterogeneities, should be made from the tangential displacement.

We now consider the case of a more complex and realistic medium where the upper crust is made up of several layers. The particular model chosen is shown in Table 1 and includes inelastic attenuation. The earthquake source is unchanged. The ground displacement computed at the same distance range as in Figure 2 is displayed in Figure 4, and the corresponding ground velocities are depicted in Figure 5.

TABLE 1

MODEL OF THE UPPER CRUST USED IN THIS STUDY

Layer	Thickness	α	β	ρ	Q_s	Q_p
1	1.5	4.0	2.3	2.6	100	140
2	3.0	5.5	3.2	2.8	200	400
3	∞	6.3	3.65	2.9	300	600

There is a striking difference between the synthetics obtained at very close range and at 25 km distance. At very near distances, velocity waveforms are very impulsive. The high-amplitude *S* or *SP* pulse is made up of two spikes of energy closely spaced in time and representing the start and stopping of the rupture [see Archuleta and Hartzell (1981) for a discussion of these phases]. At 25 km, this impulsive character has disappeared. The high-frequency energy is spread evenly over several seconds, and no single energy arrival prevails. A remarkable feature of the results is the very rapid decay of radial motion with distance from the source. This component which is the prominent one at 2 km becomes even smaller than the vertical displacement at 25 km.

The displacement spectra are displayed in Figure 6. Their degree of complexity increases regularly with distance. The spectral shape of the transverse displacement, which in the half-space case showed little dependence on epicentral distance, is now affected by the layering although somewhat less than the other components. This strong distortion of the spectra induced by the layering has also been recognized, in the case of *SH* wave by Heaton and Helmberger (1978).

APPLICATION TO THE RADIATION FROM SMALL STRIKE-SLIP EARTHQUAKES IN CALIFORNIA

We now consider the case of a complete crustal structure. We choose the velocity model of southern California obtained by Kanamori and Hadley (1975) to which we add a low-velocity surface layer. The choice of an attenuation model is difficult because the data are sparse and inhomogeneous. They consist either of values

pertaining to the very superficial layers and inferred from measurements made with high-frequency waves or they represent average crustal evaluations obtained from long-period data. We choose here, for the upper layer, the values $Q_p = 140$ and $Q_s = 100$, obtained by Bakun (1970) in central California. Between 1.5 and 3 km, we take $Q_p = 400$, $Q_s = 200$ and below 3 km, we assume $Q_p = 600$, $Q_s = 300$. Finally, for the lower crust and the mantle, we take $Q_p = 1000$, $Q_s = 500$. The velocity-attenuation model is fully described in Table 2.

The source is the one previously considered with a radius of 500 m and a rupture

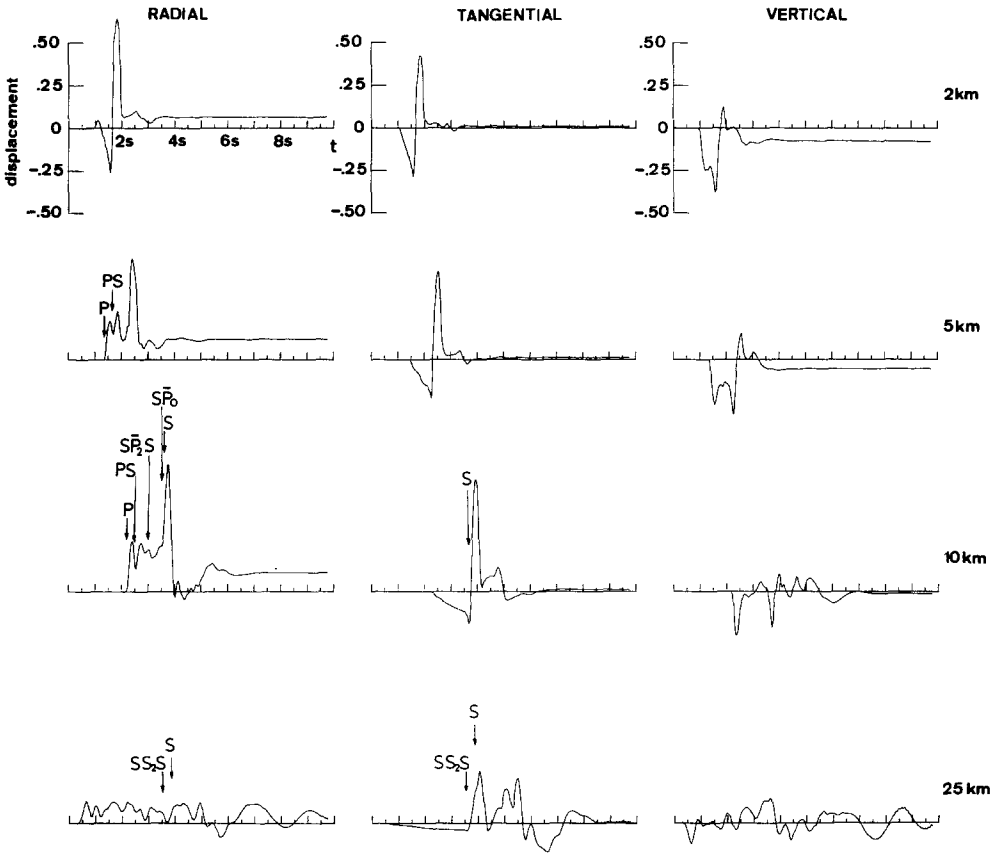

FIG. 4. Synthetic displacements for the three-layer medium with attenuation. The seismograms at 10 and 25 km have been magnified by 2 and 4, respectively. SP_i denotes the S wave which has been diffracted and has propagated with P-wave velocity along the ith interface from the surface. Amplitudes are given in centimeters for a 1-m displacement at the hypocenter.

velocity equal to 0.75β. We compute the resulting ground motion along a profile lying at 60° from the fault plane. The receiver sites span the epicentral distance range from 10 to 100 km, at 10-km intervals. Four different hypocentral depths—4, 6, 8, and 10 km—are considered. The frequency range extends from 0 Hz (static) to 5 Hz. The resulting ground velocities are shown in Figure 7. The amplitudes are given in centimeters per second for a 1-m displacement at the hypocenter. The ground motion is the superposition of many disturbances. The relative importance of each phase depends on the epicentral distance and the source depth. Some of the reflected arrivals have amplitude comparable to the direct disturbances. This is particularly true for distance beyond 70 km for which the shear wave reflected on

the Moho is the largest arrival. This wave, which at larger distances becomes part of the *Lg* wave train, is incident on the Moho at an angle of incidence more grazing than the critical angle. Its energy is consequently trapped within the crust which results in its large amplitude. The degree of complexity of the waveforms increases with the distance range. The amplitude of the Love and Rayleigh waves is strongly affected by the source depth.

The dependence of peak horizontal and vertical velocities on epicentral distance

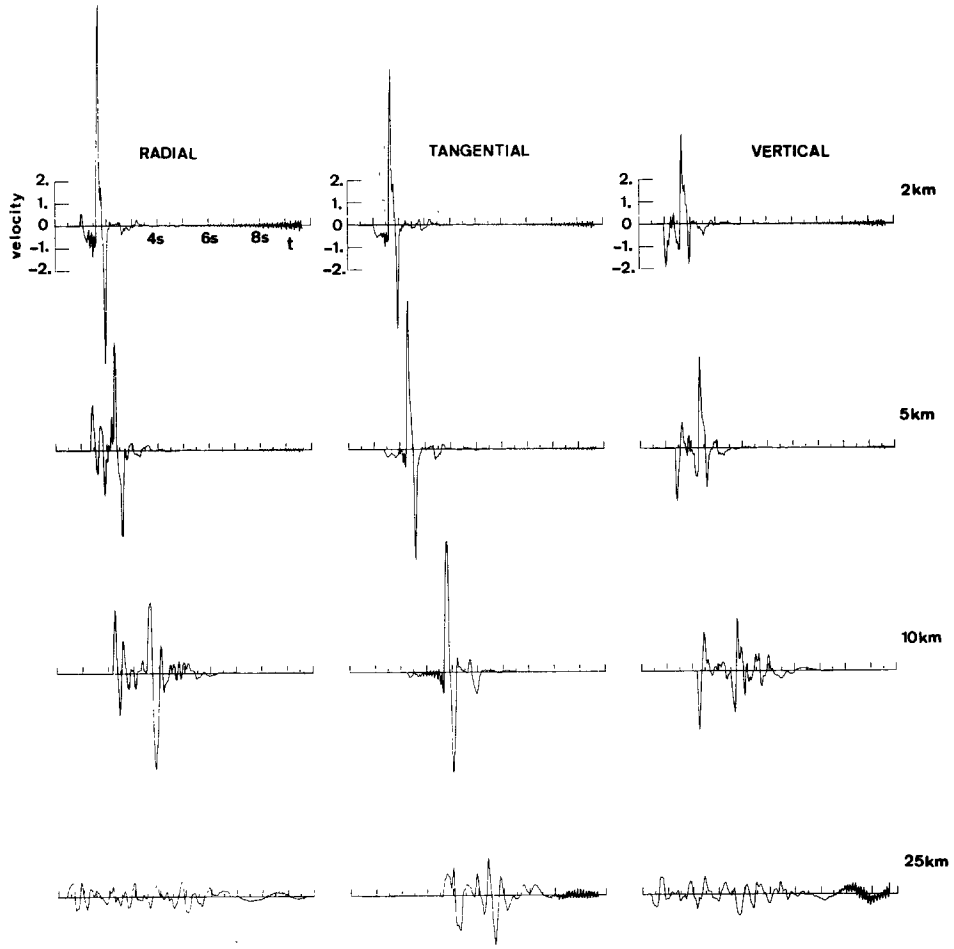

FIG. 5. Synthetic velocities for the three-layer medium. Same magnification as in Figure 4. Amplitudes are given in centimeters per second for a 1-m displacement at the hypocenter.

is displayed in Figure 8. The four different source depths are considered. The curves obtained obey a common pattern characterized by a regular decrease of amplitude up to a distance of about 80 km followed by a slight increase between 80 and 100 km. This amplitude increase starts a little beyond the critical distance for the shear wave reflected at the Moho and represents the strengthening of this reflected phase. The predominance of the supercritically reflected arrivals beyond epicentral distances of 70 to 80 km and the accompanying change in apparent geometrical spreading have also been recognized by Herrmann (1979). The rate of decrease of peak velocity in the 10 to 80 km distance range depends on the particular component considered. The tangential velocity, which has the largest amplitude, displays a

dependence of the form

$$V_{4\,\mathrm{km}} \sim r^{-1.25}$$

$$V_{6,8,10\,\mathrm{km}} \sim r^{-1.65}.$$

The slowest decrease of peak tangential velocity is obtained for the shallow source. The dependence of vertical peak velocity on epicentral distance is of the form

$$V \sim r^{-1.3}.$$

TABLE 2

CRUSTAL MODEL USED IN THIS STUDY

Layer	Thickness	α	β	ρ	Q_s	Q_p
1	1.5	4.0	2.3	2.6	100	140
2	3.0	5.5	3.2	2.8	200	400
3	23.0	6.3	3.65	2.9	300	600
4	5.0	6.8	3.9	3.1	500	1000
5	∞	7.8	4.5	3.2	500	1000

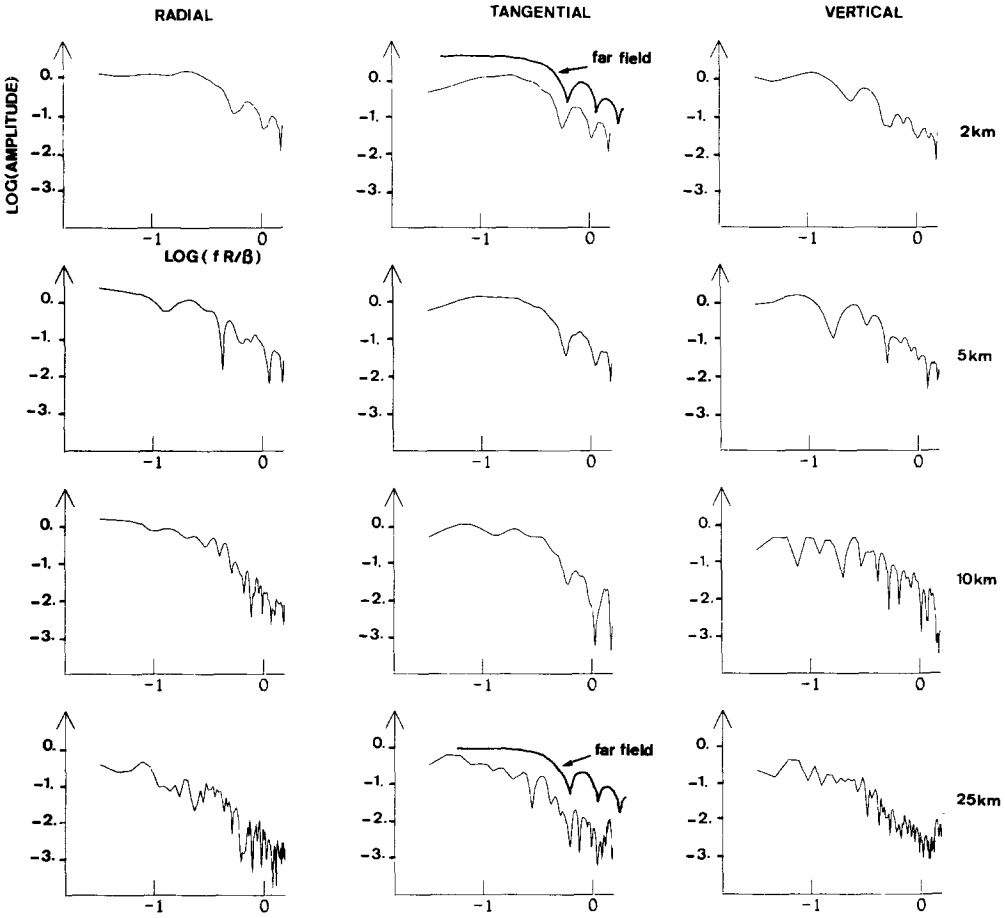

FIG. 6. Displacement spectra for the three-layer medium. The scale is the same as in Figure 3. The far-field S-wave displacement spectrum is shown for comparison.

The peak radial velocity decreases the fastest

$$V \sim r^{-2}.$$

It is interesting to compare these variations with the empirical relations deduced from observations. In doing so, one must remember that these empirical relations

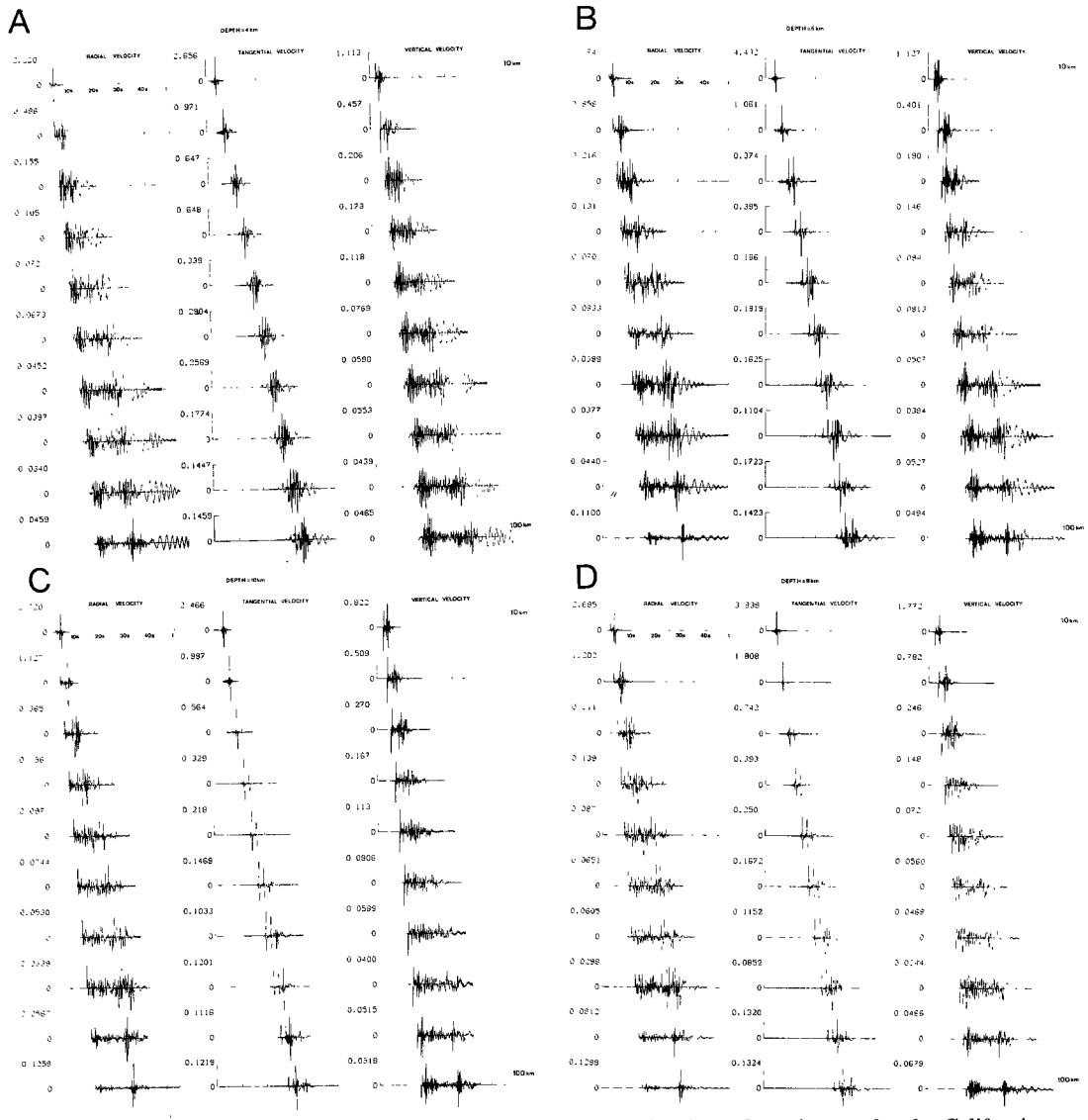

FIG. 7. (A) to (D) Ground velocity in the range 10 to 100 km from the epicenter for the California crust model. The source depth is given on each figure. Amplitudes are given in centimeters per second for a 1-m displacement at the hypocenter.

are mostly based on data obtained for large or intermediate-size earthquakes and involve different types of source mechanisms. For the San Fernando, California, earthquake of 1971, Espinosa (1977) finds a dependence of the form

$$V \sim r^{-1.35}.$$

The study by Joyner and Boore (1981), which is mostly based on California data, yields, for epicentral distances between 10 and 100 km and earthquakes around magnitude 5, a peak velocity variation of the form

$$V \sim r^{-1.2}.$$

The results of our computation are compatible with these empirical relations.

The three components of ground motion at a site completely define the translation motion but say nothing about differential motions such as strain, tilt, and rotation. To infer those, one needs to know the phase velocity of the waves which cause the motion. This can be achieved by looking at the ground motion in the frequency-horizontal wavenumber domain as shown in Figure 9. The three plots on this figure represent the spectral amplitudes of the three components of displacement for a source depth of 4 km and an epicentral distance equal to 10 km. As before, the azimuth considered is 60° with respect to the fault plane. The spectral density presents a large number of maxima. Most of the maxima are associated with phase

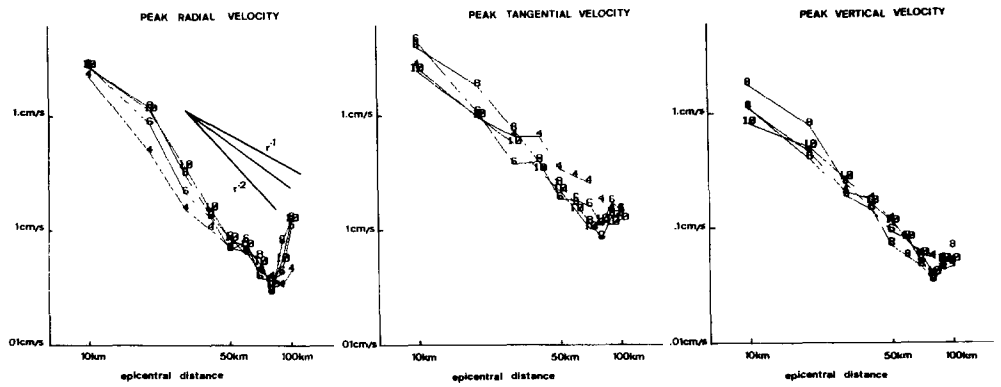

FIG. 8. Peak ground velocity as a function of epicentral distance. The numbers indicate the depth of the foci.

velocities lying between the *S*-wave velocities in the source layer and in the bottom crustal layer. For the vertical and radial components, there are also maxima close to the *P*-wave velocities. The important observation is that no significant amount of energy travels at phase velocities lower than the source-layer shear-wave velocity. The spectral amplitude of the vertical displacement at an epicentral distance of 100 km is shown in Figure 10A. The maxima occur at the same phase velocities as at a distance of 10 km. The effect of source depth is illustrated in Figure 10B. The hypocentral depth considered is 10 km and, as in Figure 9, the receiver is at 10 km from the epicenter. The source is now in the third crustal layer which results in a shift of the spectral maxima toward higher phase velocities. The source-layer shear-wave velocity is still the lower limit of the phase velocities of the disturbances which produce the ground motion.

This corroborates the results of calculations done by Luco and Sotiropoulos (1980). In the case of extended earthquake faults, Bouchon and Aki (1982) have shown that phase velocities are controlled by the basement-rock shear-wave velocity and the rupture velocity. These results show that, in the absence of lateral inhomogeneities, the amplitude of differential motions is not sensitive to the presence of low-velocity near-surface material.

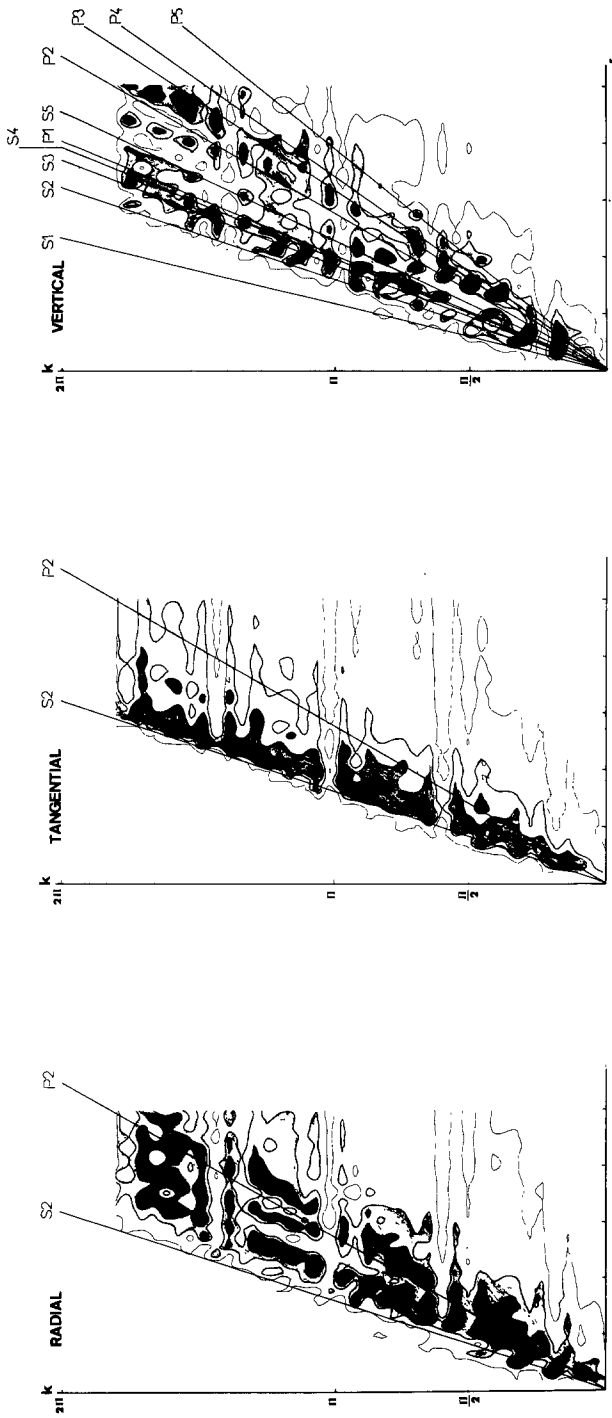

FIG. 9. Energy density in the frequency (f)-horizontal wavenumber (k) domain for the three components at 10 km from the epicenter and for a 4 km deep focus. The straight lines represent P- and S-wave velocities in the layers numbered from the top. The increase in shade denotes an increase in energy density. The curves are plotted for the values of energy density: 10^{-3}, 5×10^{-4}, and 10^{-4}.

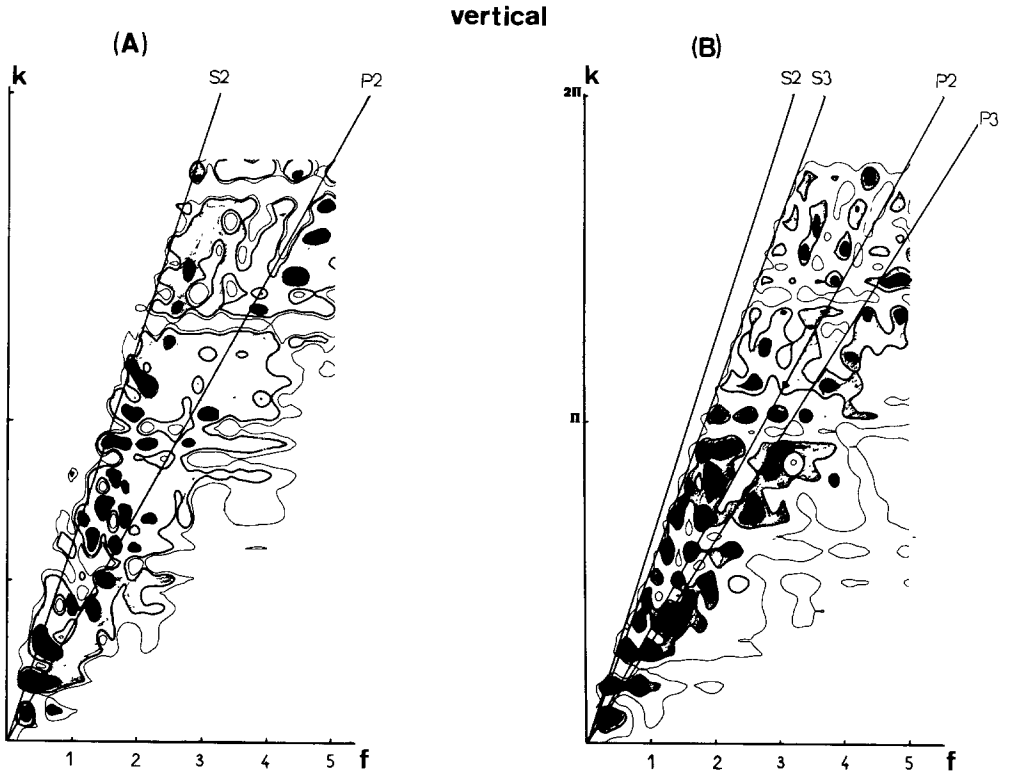

FIG. 10. (A) Density spectrum of vertical displacement in the case of a source depth of 4 km and a receiver at epicentral distance of 100 km. The curves are plotted for the values of energy density: 10^{-4}, 5×10^{-5}, and 10^{-5}. (B) Density spectrum of vertical displacement in the case of a source depth of 10 km and a receiver at epicentral distance of 10 km. The scale is the same as in Figure 9.

CONCLUSIONS

In this paper, we have tried to show that present-day numerical modeling techniques allow the complete calculation of the seismic radiation of physically realistic source models embedded in vertically heterogeneous media. The use of such techniques, in microseismicity or aftershocks studies, should lead to a more accurate determination of the source spectral parameters and allow more information about the source to be retrieved from the records.

The particular source model that we have considered here is the one of an expanding circular crack which stops suddenly, developed by Madariaga (1976). We have shown that the presence of the free surface and crustal layering strongly affects the characteristics of the radiated spectra. The spectral corner frequency, for instance, changes with epicentral distance and depends on the particular component of motion considered.

We have used this source model to calculate the decay of peak ground velocity with epicentral distance for small strike-slip earthquakes in California. Between 10 and 80 km, peak horizontal velocity decreases as $r^{-1.25}$ in the case of a 4-km hypocentral depth and as $r^{-1.65}$ for deeper sources. The predominance of supercritically reflected arrivals beyond 70 to 80 km results, for most of the cases studied, in an increase in peak ground velocity between 80 and 100 km.

ACKNOWLEDGMENTS

We thank Raul Madariaga, David Boore, and William Ellsworth for their comments. This work was supported by Institut National d'Astronomie et de Géophysique through the A.T.P. Sismogenèse.

References

Aki, K. (1966). Generation and propagation of *G* waves from the Niigata earthquake of June 16, 1964, *Bull. Earthquake Res. Inst., Tokyo Univ.* **44,** 23–88.

Aki, K., M. Bouchon, B. Chouet, and S. Das (1977). Quantitative prediction of strong motion for a potential earthquake fault, *Ann. Geofis.* **XXX,** 341–368.

Archuleta, R. and S. Hartzell (1981). Effects of fault finiteness on near source ground motion, *Bull. Seism. Soc. Am.* **71,** 939–957.

Bakun, W. H. (1970). Body-wave spectra and crustal structure: an application to the San Francisco Bay region, *Ph.D. Thesis,* University of California, Berkeley, 124 pp.

Bouchon, M. (1978). A dynamic source model for the San Fernando earthquake, *Bull. Seism. Soc. Am.* **68,** 1555–1576.

Bouchon, M. (1981). A simple method to calculate Green's functions for elastic layered media, *Bull. Seism. Soc. Am.* **71,** 959–971.

Bouchon, M. and K. Aki (1982). Strain, tilt and rotation associated with strong motion in the vicinity of earthquake fault, *Bull. Seism. Soc. Am.* **72,** 1717–1738.

Boatwright, J. (1980). A spectral theory for circular seismic sources; simple estimates of source dimension, dynamic stress drop and radiated seismic energy, *Bull. Seism. Soc. Am.* **70,** 1–28.

Espinosa, A. F. (1977). Partical velocity attenuation relations: San Fernando earthquake of February 9, 1971, *Bull. Seism. Soc. Am.* **67,** 1195–1214.

Heaton, T. H. and D. V. Helmberger (1978). Predictability of strong ground motion in the Imperial Valley: modeling the *M* 4.9, November 4, 1976 Brawley earthquake, *Bull. Seism. Soc. Am.* **68,** 31–48.

Helmberger, D. V. and S. D. Malone (1975). Modeling local earthquakes as shear dislocations in a layered half-space, *J. Geophys. Res.* **80,** 4881–4888.

Helmberger, D. V. and L. R. Johnson (1977). Source parameters of moderate size earthquakes and the importance of receiver crustal structure in interpreting observations of local earthquakes, *Bull. Seism. Soc. Am.* **67,** 301–313.

Herrmann, R. B. (1979). *SH*-wave generation by dislocation sources—A numerical study, *Bull. Seism. Soc. Am.* **69,** 1–15.

Israel, M. and R. L. Kovach (1977). Near-field motions from a propagating strike-slip fault in an elastic half-space, *Bull. Seism. Soc. Am.* **67,** 977–994.

Johnson, L. R. and T. V. McEvilly (1974). Near-field observations and source parameters of Central California earthquakes, *Bull. Seism. Soc. Am.* **64,** 1855–1886.

Joyner, W. B. and D. M. Boore (1981). Peak horizontal acceleration and velocity from strong-motion records including records of the 1979 Imperial Valley, California, earthquake, *Bull. Seism. Soc. Am.* **71,** 2011–2038.

Kanamori, H. and D. Hadley (1975). Crustal structure and temporal velocity change in Southern California, *Pure Appl. Geophys.* **113,** 257–280.

Kostrov, B. V. (1964). Self-similar problems of propagation of shear cracks, *J. Appl. Math. Mech.* **28,** 1077–1078.

Luco, J. E. and D. A. Sotiropoulos (1980). Local characterization of free-field ground motion and effect of wave passage, *Bull. Seism. Soc. Am.* **70,** 2229–2244.

Madariaga, R. (1976). Dynamics of an expanding circular fault, *Bull. Seism. Soc. Am.* **66,** 639–666.

Thatcher, W. and T. C. Hanks (1973). Source parameters of southern California earthquakes, *J. Geophys. Res.* **78,** 8547–8576.

Laboratoire de Géophysique Interne
I.R.I.G.M.
Université de Grenoble
BP 53 X 38041 Grenoble, France

Manuscript received 9 February 1982